Probing Solid-State Nanopores with Light for the Detection of Unlabeled Analytes

Brett N. Anderson[1], Ossama N. Assad[2], Tal Gilboa[2], Allison H. Squires[1], Daniel Bar[2] and Amit Meller[1,2]

[1]Department of Biomedical Engineering

Boston University

Boston, Massachusetts 02215

U.S.A.

[2]Department of Biomedical Engineering

The Technion – Israel Institute of Technology

Haifa, Israel 32000

SUPPLEMENTARY INFORMATION

1. Rhod-2 - Ca^{2+} binding constant measurements for different EGTA concentrations

Calcium chloride was titrated into a volume of 1M KCl to the final concentrations as indicated in Fig. S2. The concentration of Rhod-2 concentration was fixed at 5.6 μM, and fluorescence was measured at the confocal spot, positioned 100 μm above a glass coverslip. The experiment was repeated for three EGTA concentrations (10, 50, and 100 mM EGTA). The midpoint of each curve between background fluorescence and saturation was termed the k_D for a given concentration of EGTA which competes for calcium binding with the calcium indicator Rhod-2. Higher concentrations of EGTA shift the midpoints toward higher concentrations of $CaCl_2$.

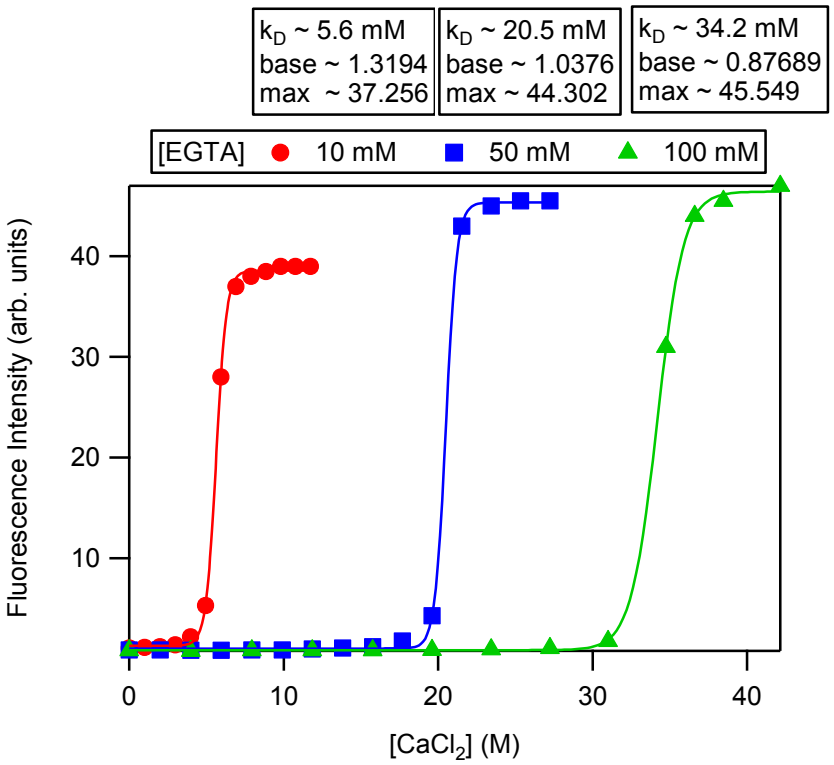

Figure S2 | Measurements of Rhod-2 - Ca^{2+} binding constants at different EGTA concentrations. Curves show the fluorescence intensity of Rhod-2 under excitation of 532 nm laser *vs.* calcium chloride and EGTA concentrations, and a fixed Rhod-2 concentration.

2. Fluorescence intensity *versus* voltage curves at different $CaCl_2$ concentrations (*trans*) and EGTA concentrations (*cis*).

A 4 nm nanopore was assembled in the optical setup and illuminated using green laser (λ_{exc} = 532 nm). Continuous I_f - V curves were taken as the voltage was ramped from -1V to 1V in 0.01 V increments, for 0, 10, 50, 100, 500, 1000, and 3000 mM calcium chloride (*trans*) and EGTA concentrations as indicated in the *cis* chamber.

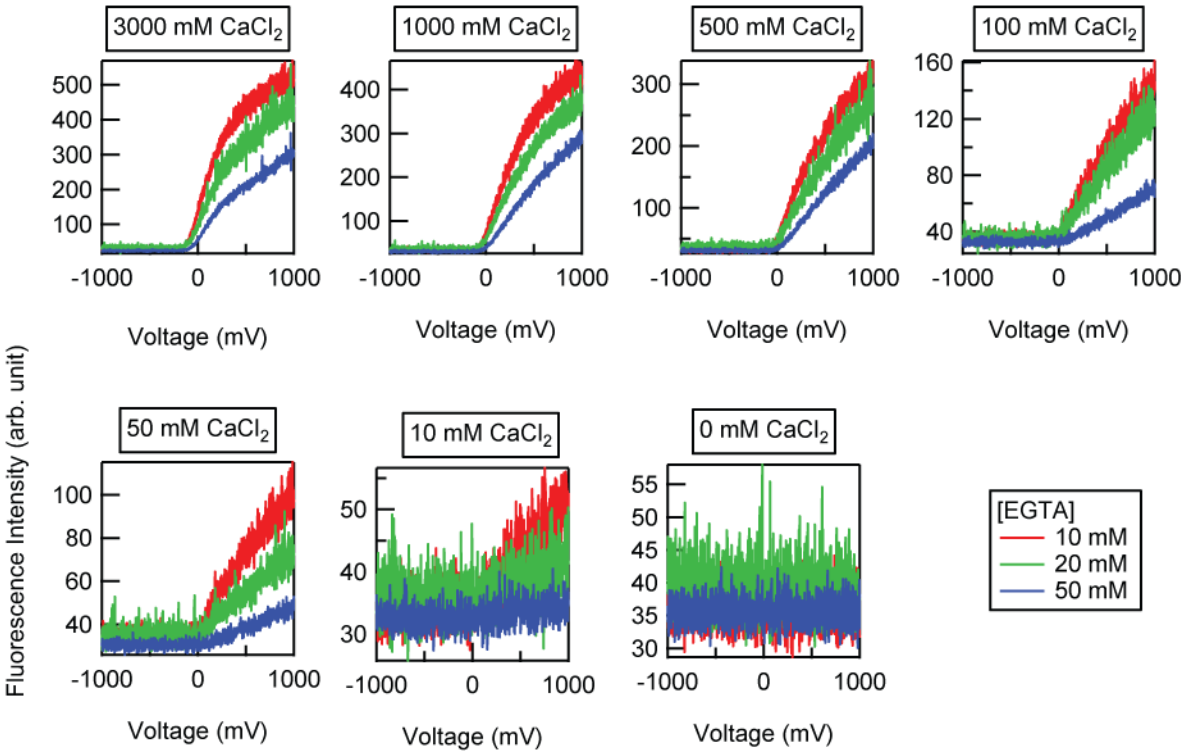

Figure S3 | Fluorescence intensity *vs.* voltage for 0, 10, 50, 100, 500, 1000, and 3000 mM $CaCl_2$ in 10, 20, and 50 mM EGTA, measured using a 4 nm solid-state nanopore.

A summary of the data shown in Figure S3 is given in Figure S4 using the same Y scale for the entire $CaCl_2$ concentration range (0 – 3M) at fixed [EGTA] = 10 mM.

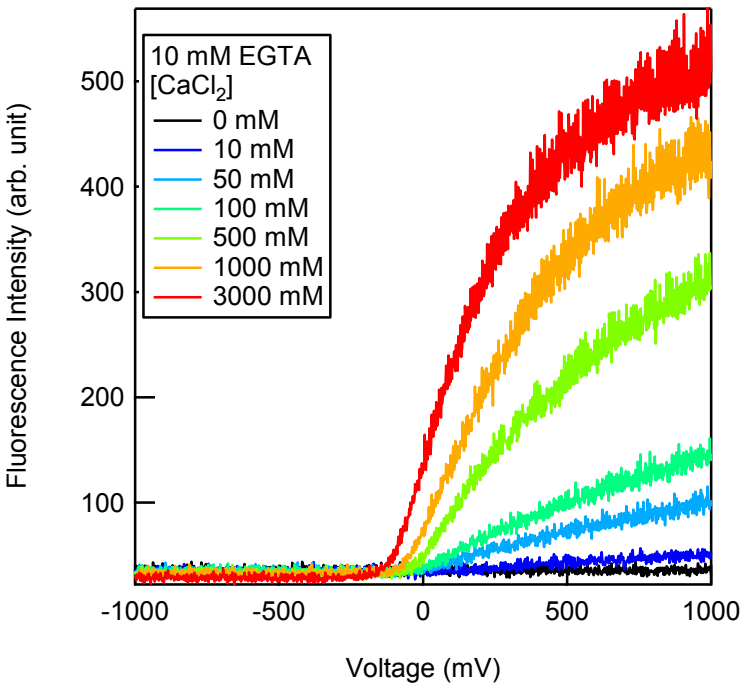

Figure S4 | Fluorescence intensity *vs.* voltage for 0-3M $CaCl_2$ in 10 mM EGTA

3. Numerical model of Ca^{2+} - bound dye concentration distributions near a solid-state nanopore.

Following previous studies[1, 2] we used the Poisson-Nernst-Planck equations to model ionic concentration distributions near nanopores. We numerically solve Poisson's equation,

$$\nabla^2 V = -\frac{F}{\varepsilon}(2c_{Ca} + c_K - c_{Cl}),$$

and the Nernst-Planck equation for each ionic species (potassium, calcium, and chloride),

$$\nabla \cdot \overrightarrow{J_{Ca}} = 0$$

$$\overrightarrow{J_{Ca}} = -D_{Ca}\nabla c_{Ca} - z_{Ca}\mu_{Ca}F c_{Ca}\nabla V$$

$$\nabla \cdot \overrightarrow{J_K} = 0$$

$$\overrightarrow{J_K} = -D_K\nabla c_K - z_K\mu_K F c_K \nabla V$$

$$\nabla \cdot \overrightarrow{J_{Cl}} = 0$$

$$\overrightarrow{J_{Cl}} = -D_{Cl}\nabla c_{Cl} - z_{Cl}\mu_{Cl}\mathrm{F}c_{Cl}\nabla V,$$

where *V* is the electric potential, *F* is the Faraday constant (~96,485 s·A/mol), ε is the dielectric constant permittivity of water (~$7.09{\cdot}10^{-10}$·m^{-3}·kg^{-1}·s^4·A^2), and c_i is the concentration, $\vec{J}$ is the flux, D_i is the diffusion constant, z_{Ca} is the charge number, and μ_{Ca} is the electrophoretic mobility of each ion species *i*. The diffusion constant D_i is calculated from the Einstein-Smoluchowski relation,[3]

$$D_i = \frac{\mu_i k_B T}{q}$$

where k_B is the Boltzmann constant, *T* is the temperature, and *q* is the electric charge of each ion species. The boundaries are set to 1 μm in all directions around the pore forming a sphere of radius 1 μm in a 2D axisymmetric model (**Fig. S5**). The boundaries in *cis* and *trans* are set to constant concentrations and the far and near boundaries are set to 0 V (in *cis*) and a target voltage in *trans*. These are reasonable approximations as the *cis* and *trans* chambers in the experiment are large enough to be taken as constant concentration sources relative to the duration of an experiment.

We solve for equilibrium spatially distributed steady-state free calcium in the presence of the chelating agent EGTA[4] according to

$$[Ca] = [C_T] - \tfrac{1}{2}([C_T] + [EGTA] + k_D - \sqrt{-4[C_T][\mathrm{EGTA}] + ([C_T] + [\mathrm{EGTA}] + k_D)^2})$$

where k_D = 150 nM is the dissociation constant for EGTA-Ca[5], $[C_T]$ is the total calcium concentration (numerically solved for with PNP), and $[EGTA]$ is the concentration of EGTA. We solve for the concentration of calcium-bound Fluo-4 (again, following ref 4) according to

$$[F \cdot Ca] = \tfrac{1}{2}([\mathrm{C}] + [F] + k_D - \sqrt{-4[Ca][\mathrm{F}] + ([Ca] + [F] + k_D)^2},$$

where k_D of Fluo-4 for Ca is 345 nM[6] and [Fluo-4] is an experimentally determined concentration.

To model the total intensity acquired with TIRF illumination mode, we calculated the evanescent *I(z)* using:

$$I(z) = I_0 e^{-z/\delta}$$

with a skin depth δ

$$\delta = \frac{\lambda}{4\pi\sqrt{{n_1}^2 sin^2\theta - {n_2}^2}} \sim 100\ nm$$

where n_1 is the index of refraction of the *trans* chamber, n_2 is the index of refraction of the *cis* chamber, and θ is the angle of incidence of the 488 nm excitation laser from *cis* to *trans*. We then integrate for total fluorescence (*F*):

$$F = k \int_0^L I(z)[F \cdot Ca](z)dz$$

where *L* is 100 μm, the distance to the *cis* boundary in our numerical model.

The simulations were run with the potential difference across the pore ramped from -1V to 1V in 50 mV steps for each concentration of $CaCl_2$. We then calculated F for each voltage and $CaCl_2$ concentration and used the parameter k to scale the theoretical curves to the experimentally measured value at 1V. We note that the simulations are only simple approximations to the experimentally observed values, however, they replicate quite clearly the same trends (*e.g.*, both show sigmoidal saturating behavior at similar voltages and fluorescence intensity scaling with $CaCl_2$). Furthermore, while it would be difficult to calculate real fluorescence intensity numbers given that many experimental parameters are lumped into *k* (photon counts/second for a given experimental conditions *a priori*), our models clearly show that the gradient of the calcium-bound fluorophore can be finely tuned in understandable ways by varying $CaCl_2$, EGTA, and Rhod-2 or Fluo-4 concentrations, or by varying the voltage, within the range of several nanometers to micrometers with variable decay rates, and are thus valuable guides to experiments.

4. Asymmetric *trans/cis* calcium concentration increases capture rate and slows translocation

Asymmetric distributions of calcium chloride, with $CaCl_2$ in *trans*, were shown to both increase capture rate (**Fig. S5**) and slow down translocations (**Fig. S6**) without substantially changing the normalized blockade (**Fig. S7**) levels for 1 kbp DNA at 300 mV in a 4 nm pore relative to similar KCl gradients.

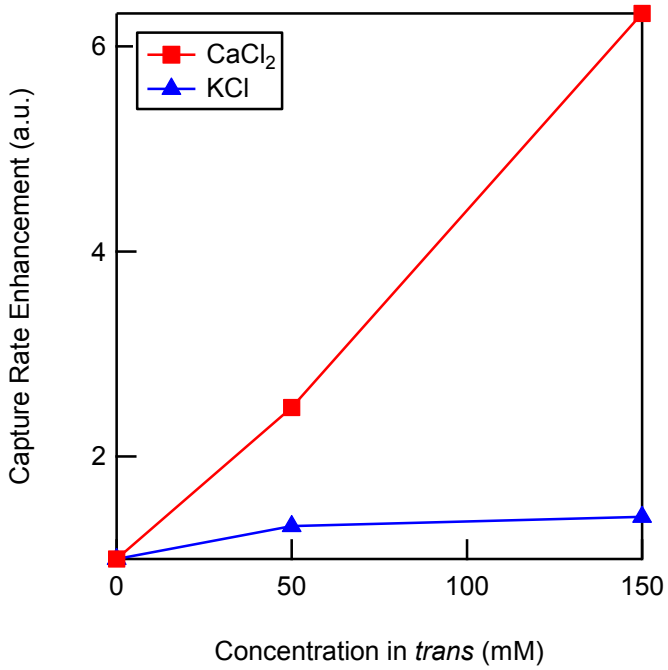

Figure S5 | Capture rate enhancement of 1 kbp DNA in a 4 nm pore with $CaCl_2$ and KCl gradients.

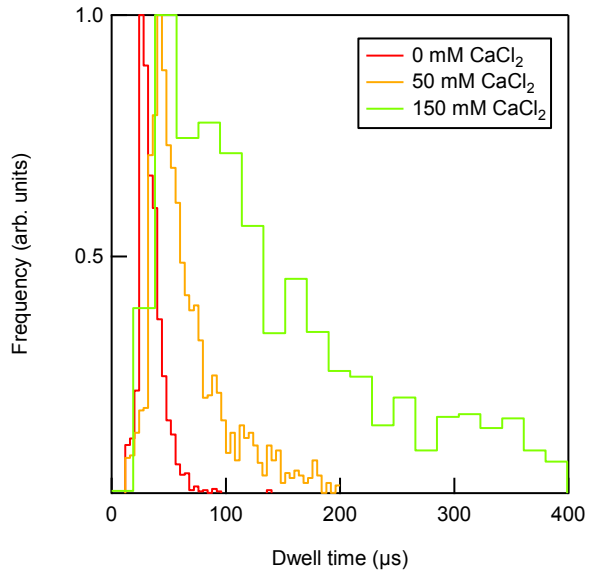

Figure S6 | Increasing calcium chloride concentration in *trans* incrementally slows down DNA translocation (1 kbp DNA, 4 nm pore, V = 300 mV).

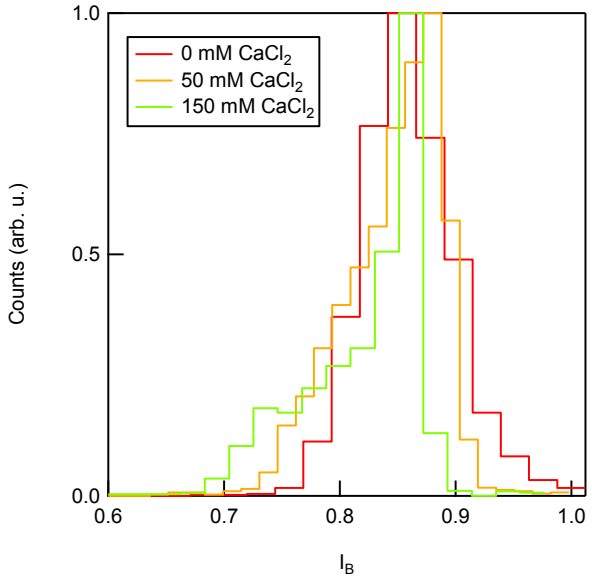

Figure S7 | I_B for translocation shows similar peak blockage levels at three concentration of *trans* $CaCl_2$ (1 kbp DNA, 4 nm pore, V = 300 mV).

5. Synchronous electrical and optical translocation blockade depth

Synchronous electrical and optical translocations of 1 kbp, 8 kbp, and 10 kbp DNA at 300 mV are shown in **Fig. S8**.

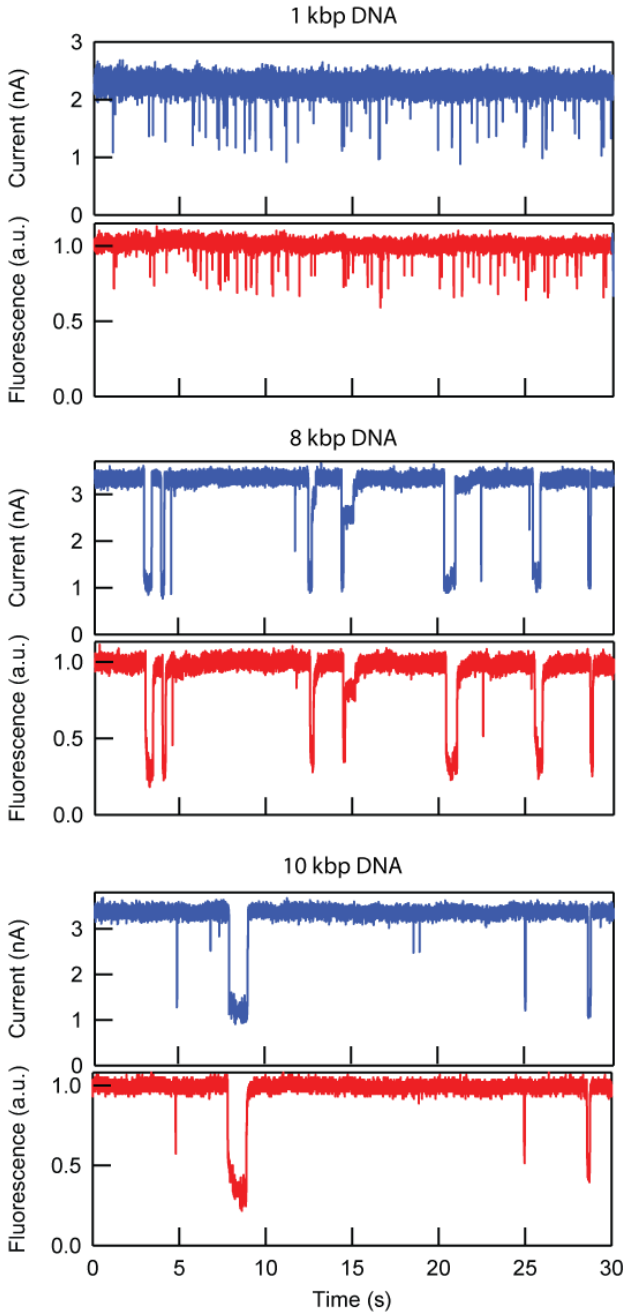

Figure S8 | 1 kbp, 8 kbp, and 10 kbp (~1.5 nM, ~192 pM, and 154 pM, respectively) synchronous electrical and optical translocation at 300 mV in 4 ± 0.2 nm pores with 4 μM Fluo-4 in *cis* and 250 mM $CaCl_2$ in *trans*.

6. Comparison of Electrical *versus* Optical noise during long DNA translocations.

We compared the blocked level noise in the ion currents to those in the optical signal for a set of long DNA translocations (t_D > 10 ms, N = 57). These events were acquired using a 8 kbp DNA, 2.8 nm pore at V = 1V). Electrical and optical events were acquired simultaneously, and for each event we measured the width at half maximum of the relative blocked ion current distributions during translocations. Our results (shown in **Fig. S9**) indicate that the optical signal as whole displayed more consistent average blocked levels, and a smaller dispersion overall than the electrical signal (the standard deviations in normalized blockade levels were 0.064 and 0.033, for the mean I_B and F_B of all events, respectively). This is consistent with the absence of flicker low frequencies noise in the spectrum of the optical signal, and may offer a significant improvement over electrical sensing when accurate determination of a current level is necessary.

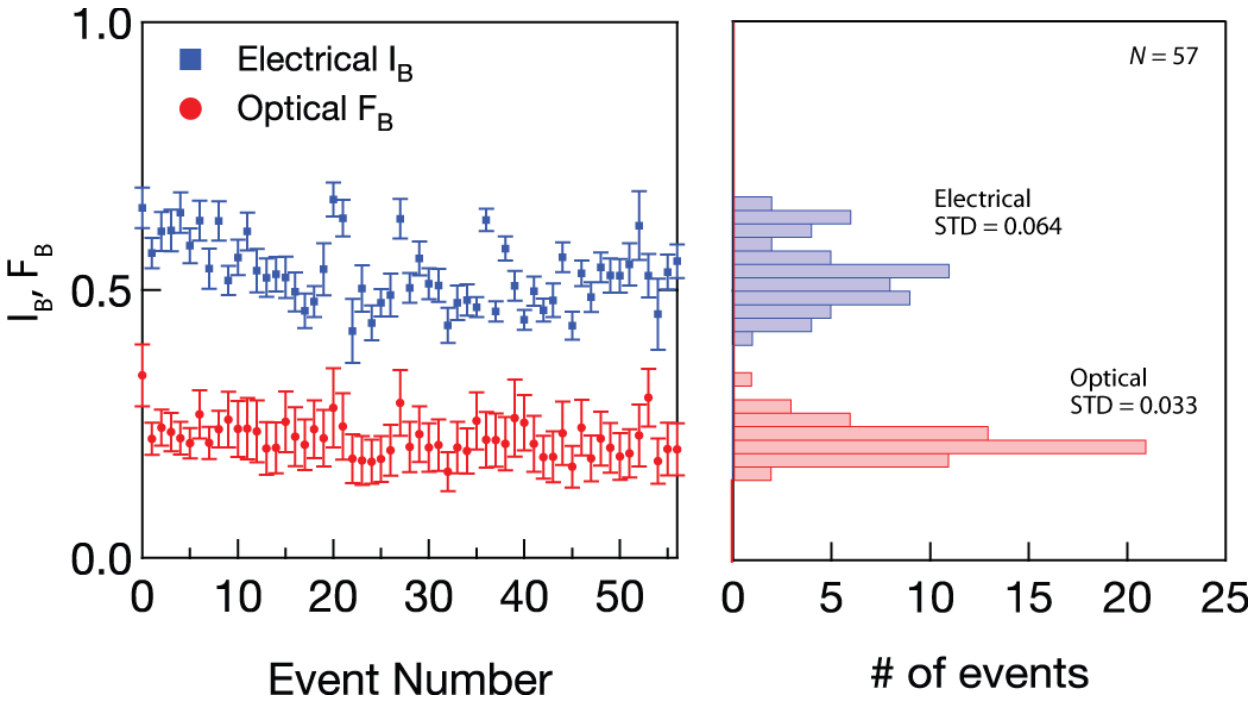

Figure S9 | 8 kbp DNA blockades at 1 V in a 2.8 nm pore with 250 mM $CaCl_2$ in *trans* and 20 μM Fluo-4 in *cis*. Left panel: the electrical (I_B and optical F_B) fractional blocked levels for all events. Right panel: histograms of all events using equal bins, showing a narrower distribution for the optical signals of the same events.

7. Experimental Setup

A schematic of the optical and electrical components of the experiment is shown in Fig. S10. Both confocal and TIRF modes can be used with two different laser lines, as explained in the

text. Abbreviations: PD, Photo-diode; Pol, Half-wavelength wave plate; DM, Dichroic Mirror; NF, Notch Filter; PH, Pinhole; APD, Avalanche Photo-Diode; PZT-NP, Piezo-Nanopositioner; CNT, Counter source; AI, Analog Input; AO, Analog output.

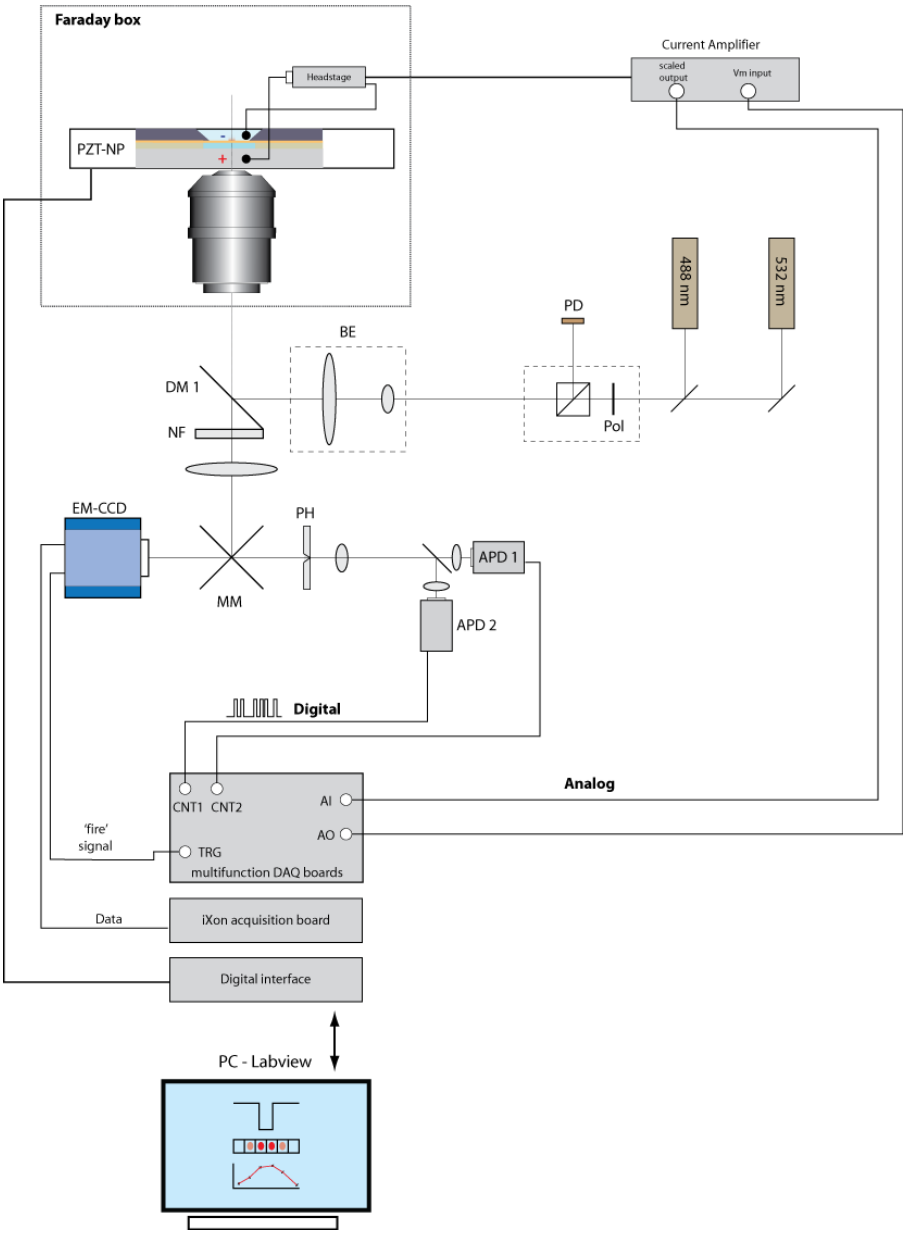

Figure S10 | Optical and electrical experimental setup schematic

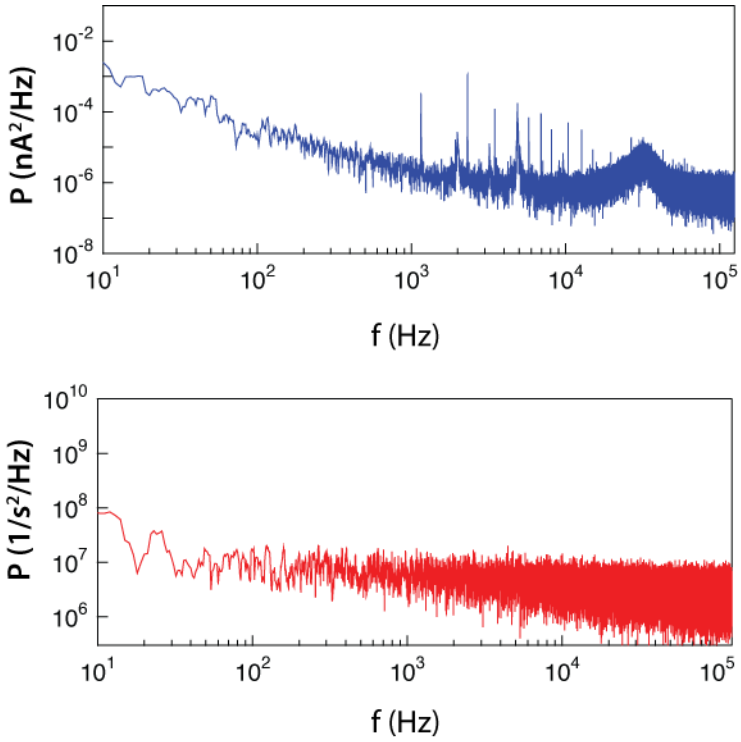

Figure S11 | Electrical and optical measurements of Power Spectrum Distributions, measured simultaneously using 75 mM Ca^{2+}, V =300 mV and 400 µM Rhod-2 (electrical signal filtered at 40 KHz using Butterworth filter).

SUPPLEMENTARY REFERENCES

1. Wanunu, M., Morrison, W., Rabin, Y., Grosberg, A.Y. & Meller, A. Electrostatic Focusing of Unlabelled DNA into Nanoscale Pores Using a Salt Gradient. *Nat. Nanotechnol.* 2010, 5, 160-165.
2. Powell, M.R. et al. Nanoprecipitation-Assisted Ion Current Oscillations. *Nat. Nanotechnol.* 2008, 3, 51-57.
3. Dill, K.A. & Bromberg, S. Molecular Driving Forces : Statistical Thermodynamics in Chemistry and Biology; Garland Science: New York, 2003.
4. Hulme, E.C. & Trevethick, M.A. Ligand Binding Assays at Equilibrium: Validation and Interpretation. *Brit. J. Pharmacol.* 2010, 161, 1219-1237.
5. Qin, N., Olcese, R., Bransby, M., Lin, T. & Birnbaumer, L. Ca2+-Induced Inhibition of the Cardiac Ca2+ Channel Depends on Calmodulin. *Proc. Natl. Acad. Sci. U S A* 1999, 96, 2435-2438.
6. Gee, K.R. et al. Chemical and Physiological Characterization of fluo-4 Ca^{2+}-Indicator Dyes. *Cell Calcium* 2000, 27, 97-106 .